Annual report: BCOGRIS EI-2016-09, year 1
Fluid Mechanic Causes of Gas Migration

BACKGROUND

A significant % of oil & gas wells leak, allowing gas and subsurface fluids to migrate to surface. This is despite >80 years of worldwide experience in primary cementing of oil & gas wells, together with significant evolution of industry no-how, equipment and materials. Leakage is common in Western Canada and presents environmental and health/safety risks, as well as reducing well productivity. Key reasons for the failure of the industry to solve this problem include both managerial/operational factors and the wide range of different potential physical causes.

This project initiates an in depth study of those physical causes related to fluid mechanic issues, with the aim of improving physical understanding in the industry. Three areas were highlighted for attention, using a mix of analytical, computational and experimental techniques.

- ***Micro-annulus formation and prevention during cement placement***
- ***Fluid invasion into a gelled column.***
- ***Cement hydration modelling and predicting pore pressure reduction.***

SUMMARY OF ACTIVITIES & RESULTS

Main activities in the 3 areas were as follows

- ***Micro-annulus formation and prevention during cement placement***

In primary cementing the cement slurry is usually preceded by one or more washes/spacer fluids, which are designed to have a rheology and density that aids displacement of the drilling mud from the narrow annular space. However, due to the yield stress and viscosity of the drilling mud, it is common that a part of the mud is left behind on the walls. These thin layers may connect around the circumference forming a so-called micro-annulus. These residual mud layers may form the basis for longitudinal conduits of porous de-hydrated mud, after the cement has set, allowing migration of gas and other reservoir fluid.

Since more than 10 dimensionless parameters are involved in the displacement of 2 non-Newtonian fluids with yield stress in a 3D annular geometry, our initial approach is to simplify to a 2D longitudinal section of the narrow annulus, at fixed azimuth. We consider this section to be vertical (e.g. surface casing). We model only the simplest yield stress fluid (Bingham fluid) as the drilling mud – the yield stress is the key cause of the mud layers, and simplify the spacer rheology by considering it Newtonian. This reduces the dimensionless parameter set to 5 parameters: Reynolds (Re), Froude (Fr), Atwood (At) and Bingham (B) numbers, plus viscosity ratio (m). We study only density stable displacements, as the annular fluids typically obey a density hierarchy. The limit of small Atwood number is also imposed, in which the effects of buoyancy on accelerations is eliminated, thus reducing to a 4 parameter system.

We have modelled this system computationally, running 100's of simulations over significant parameter ranges (Re,Fr,B,m). The main findings are

- Buoyancy increases the efficiency of residual mud layer removal, i.e. the (micro-annulus) mud layer thickness reduces.
- The thickness of the residual layer increases as the ratio m of the viscosity of displaced fluid to that of the displacing fluid increases.
- Interestingly, the residual layer sometimes thins on increasing the yield stress of displaced fluid. This paradoxical effect is being further explored.
- The displacement process happens over a shorter time frame at higher values of viscosity ratio and lower values of Bingham numbers. More precisely, these trends give rise to the largest ratios of front velocity compared to the mean imposed (pumping) velocity. In the wellbore context, these would lead to earlier "breakthrough" times. In this respect, the largest front velocities are found in Newtonian-Newtonian displacements with $m \approx 10$ or larger.

In parallel we have developed a semi-analytical 2-layer model that can give quick computations and predict the displacement front velocity and other features of the displacement at long times. The results of this model are being compared with the 2D computations. The aim is to characterize the different types of displacement in a buoyancy-viscosity ratio map. Currently we have identified 3 basic classifications for the displacement front: (1) frontal shock (plug type interface); (2) contact shock (spike type interface); (3) no shock (dispersive interface). In each case we may have a residual mud layer or not.

A paper is in preparation for submission based on our findings.

- ***Fluid invasion into a gelled column.***

In order for formation fluids (gas or liquid) to enter the well it is necessary for there to be a pressure imbalance. A pressure imbalance may not however be sufficient for fluids to invade. In the event of the invading fluid being immiscible with the cement slurry, it is firstly also necessary to overcome a capillary pressure limit, which may depend critically on the pore radius or other local geometry. Secondly, the rheology of the cement slurry has an effect on invasion, as is widely acknowledged in the industry, e.g. in API recommendations and in additives targeted at control of gel strength in the semi-solid slurry.

We have built and modified an experimental test cell to study the invasion process. In place of gas, to eliminate buoyancy and capillary effects, we have first worked with aqueous liquids as the invading fluid. The in situ gelled column is Carbopol, a transparent lab fluid with yield stress varied by adjusting concentration and pH. A single invasion pore is placed centrally in the bottom of the gelled column. The applied pressure (overpressure) in the invading fluid is controlled very precisely with a manometer design.

The first set of experiments involved water as the invading fluid. We observed that invasion happens following a complex sequential process with the following stages: initial mixing/diffusive stage, invasion dome stage, transition stage, soft fracture propagation. These stages have been visualized and to some extent quantified. In parallel, further insights have been gained from a computational study that shows the transition in ideal yield stress fluids from localised recirculatory patterns to a Poiseuille type motion of the entire column as the invading pressure is increased. Details of these results are included in a paper accepted for publication in the Journal of non-Newtonian Fluid Mechanics which is included as an appendix to this report.

Additional results obtained in the first year are being analyzed. These focus at the fracture stage, after invasion, where the invading fluid propagates through the gelled column. We also have a large sequence of experimental results using glycerol solutions as the invading fluid (exploring viscosity and density effects).

- ***Cement hydration modelling and predicting pore pressure reduction.***

This is a new area for the group and so far our attention has been mostly on the above two areas. We have developed a general "two-fluid" model for evolution of the solid and liquid phases in the slurry and have started reviewing literature in order to predict evolution of the cement chemistry during hydration.

We have reproduced the results in 2 model studies developed by Billingham and co-workers: (1) delayed nucleation theory; (2) Effects of retarder. In the first of these the hydration of cement is explained with a dissolution-precipitation mechanism, which involves the first two stages of reactions: pre-induction and induction. On contact with water, C_3S (alite) releases calcium and calcium hydroxide (CH) ions and a very thin layer of C-S-H forms on the surface of each of the grains. This stage is the so-called pre-induction period. According to Billingham's delayed nucleation theory, the growth of C-S-H encounters a delay (the induction period) that is modelled mathematically by assuming that the rate of chemical reactions is limited when the C-S-H concentration reaches a maximum value. These are preliminary and it is not clear yet which hydration models will form the basis for future work.

PRESENTATIONS & PUBLICATIONS

Results from the study to date have been presented in the following forums.

[1] *Gel Strength Effects on Fluid Invasion into a Cemented Annuli: Part 1*. M. Zare, L. Gassmann, I. Frigaard. Poster presented at the Unconventional Gas Technical Forum, April 4-5, 2016, Victoria, BC, Canada.

[2] *Gel Strength Effects on Fluid Invasion into a Cemented Annuli: Part 2*. M. Zare, L. Gassmann, I. Frigaard. Poster presented at the Unconventional Gas Technical Forum, April 4-5, 2016, Victoria, BC, Canada.

[3] *Invasion of fluids into a gelled fluid column: Yield stress effects*. M. Zare, A. Roustaei, K. Alba, I.A. Frigaard. Journal of Non-Newtonian Fluid Mechanics, article accepted and to appear 2016, (http://dx.doi.org/10.1016/j.jnnfm.2016.06.002).

[4] *Rheological Effects on Fluid Invasion into Cemented Annuli*. M. Zare, Q. Lindfield-Roberts, M. Ward, K. Alba, I.A. Frigaard. Poster and proceedings paper at 9th International Conference on Multiphase Flow (ICMF 2016) May 22-27, 2016 Florence, Italy. This poster was winner of the ICMF poster prize.

FUTURE ACTIVITIES & MILESTONES

In year 2 of the project we plan to continue work in all 3 areas, as follows.

- ***Micro-annulus formation and prevention during cement placement***

Here we intend to extend our modelling approach to include some of the following:

- Density unstable configurations
- Inclination of the model geometry (apart from vertical)
- Inclusion of a yield stress in the displacing fluid and potentially other rheological effects such as shear-thinning.

Our first milestone is to finish preparation of the article describing our initial results.

- ***Fluid invasion into a gelled column.***

We intend to continue our approach of experimental study of invasion supplemented by computations. In year 1 we focused at miscible invasions with no density difference (water-Carbopol). In year 2 we intend to initiate the study of gas invasion. As an interim stage we may also consider capillary effects with a density-matched immiscible invading fluid. We will start the study using a similar setup (single centrally positioned invasion hole) to compare against the year 1 results. Later we hope to prototype different geometries mimicking the wellbore setup, e.g. some form of porous wall in a gelled column. An additional milestone is to finish preparation of an article describing our results from year 1 on glycerin invasion into Carbopol.

- ***Cement hydration modelling and predicting pore pressure reduction.***

We intend to focus on this area significantly, with the aim of completing model development by Q2 2017 and deriving initial computed results from this model in Q3/Q4 2017.

TEAM

Those funded partly from this project include:

- Marjan Zare, lead researcher, PhD student responsible
- Matthew Ward, undergraduate intern UBC (Sept - Dec 2015). Contributor to fluid invasion studies
- Linus Gassmann, visiting masters student from TU Munich (Nov 2015 – April 2016). Contributor to fluid invasion studies
- Dr Ali Roustaei, Postdoc researcher giving computational support on micro-annulus formation and invasion studies

Involved in a supervisory capacity were:

- Dr I.A. Frigaard (PI, faculty member at UBC)
- Dr J. Stockie (Faculty member at Simon Fraser University) collaborating on development of the hydration model.
- Dr Kamran Alba (former postdoc and now faculty member at University of Houston) involved in initial project design and setup of the fluid invasion experiment.

BUDGET

Budget of $40,000 for year 1 of the project is spent/committed up until end of project year.

Approximate breakdown: salary costs $26,500; equipment, materials and other supplies $8,000; travel and conference expenses $5,500.

APPENDIX

Invasion of fluids into a gelled fluid column: Yield stress effects. M. Zare, A. Roustaei, K. Alba, I.A. Frigaard. Journal of Non-Newtonian Fluid Mechanics, article accepted and to appear 2016, (http://dx.doi.org/10.1016/j.jnnfm.2016.06.002).

Journal of Non-Newtonian Fluid Mechanics 000 (2016) 1–12

Contents lists available at ScienceDirect

Journal of Non-Newtonian Fluid Mechanics

journal homepage: www.elsevier.com/locate/jnnfm

Invasion of fluids into a gelled fluid column: Yield stress effects

M. Zare[a], A. Roustaei[a], K. Alba[b], I.A. Frigaard[c,*]

[a] Department of Mechanical Engineering, University of British Columbia, 2054-6250 Applied Science Lane, Vancouver, BC V6T 1Z4 Canada
[b] Department of Engineering Technology, University of Houston, College of Technology Building, 4730 Calhoun Road #304, Houston, TX 77204-4020, United States
[c] Departments of Mathematics and Mechanical Engineering, University of British Columbia, 1984 Mathematics Road, Vancouver, BC V6T 1Z2, Canada

ARTICLE INFO

Article history:
Received 31 March 2016
Revised 18 May 2016
Accepted 1 June 2016
Available online xxx

Keywords:
Well integrity
Gas migration
Yield stress fluid

ABSTRACT

We study the invasion of a Newtonian fluid into a vertical column of yield stress fluid through a small hole, using both experimental and computational methods. This serves as a simplified model for understanding invasion of gas into cemented wellbores. We find that the invasion pressure must exceed the static pressure by an amount that depends linearly on the yield stress of the fluid and that (for sufficiently deep columns) is observed to increases with the height of the yield stress column. However, invasion pressures far less than the Poiseuille-flow limit are able to yield the fluid, for sufficiently small hole sizes. Observed experimental behaviours in yielding/invasion show a complex sequence of stages, starting with a mixing stage, through invasion and transition, to fracture propagation and eventual stopping of the flow. Precise detection of invasion and transition pressures is difficult. Invasion proceeds initially via the formation of a dome of invaded fluid that grows in the transition stage. The transition stage appears to represent a form of stress relaxation, sometimes allowing for a stable dome to persist and at other times leading directly to a fracturing of the gel. The passage from initial invasion through to transition dome is suggestive of elasto-plastic yielding, followed by a brittle fracture. Computed results give qualitative insight into the invasion process and also show clearly the evolution of the stress field as we change from local to non-local yielding.

1. Introduction

Gas migration has been a chronic problem in the completion of oil and gas wells for decades [1,2]. This is a complex phenomenon with causes that combine chemical, geochemical and fluid mechanical processes. The consequences of gas migration can range from gas emissions at the wellhead or into the surrounding subsurface ecosystem, to aquifer contamination and in extreme cases to well blowouts. In addition, leakage lowers reservoir pressures impacting well productivity. Thus, gas migration impacts health and safety, environment and economic aspects of hydrocarbon energy production.

A key difficulty of understanding gas migration is that the causes manifest over different timescales in the well construction process. Here we focus on early-mid stage gas migration, which happens during the primary cementing of a well, and on rheology effects. In primary cementing [3] a steel casing is inserted into the newly drilled borehole and cement slurry is placed into the annular space surrounding the casing and bordering the reservoir. After the pumps are turned off the cement slurry is left to set within a narrow annular space (e.g. 2–6 cm mean annular gap, for mean diameters anywhere in the range 12–30 cm) that extends many 100's of meters along the wellbore. The cement slurry which generally has modest yield stress ($\sim$5–10 Pa) develops a significant gel strength during the early stages of hydration, when it may still be regarded as a semi-solid yield stress suspension. During this stage the root cause of gas invasion into the well is pressure imbalance.

There are various theories about how pressure imbalance is generated (e.g. [4–6]), but here we will simply acknowledge that it happens. The cementing industry commonly uses additives for gas migration treatment that affect rheology post-placement, i.e. generally increasing the yield stress of the slurry. Once gas has entered the wellbore and migrates upwards in the annulus, rheology certainly has a role to play in retarding or preventing propagation of bubbles/gas streams. However, at that stage the well integrity is already compromised (at least partially). Instead therefore we address the question of what are the effects of the yield stress on fluid invasion?

* Corresponding author.
E-mail address: frigaard@math.ubc.ca (I.A. Frigaard).

http://dx.doi.org/10.1016/j.jnnfm.2016.06.002

In hydrocarbon bearing rocks permeabilities vary widely, giving representative pore sizes in the μm range for conventional reservoirs, down to *nm* range for many tight/unconventional reservoirs, an example of the latter being the Montney shale found in Northeastern British Columbia [7]. For porosity ranges $\leq$ 4%, pores abutting the newly drilled borehole are essentially isolated holes on a surface. This leads us to the following problem.

Consider a tall column of static yield stress fluid with a single small “hole” in the wall of the container. We apply fluid under pressure through the hole and question whether or not the fluid invades and under what mechanism. In the case of a purely viscous fluid within the container and if we neglect capillary effects, a pressure over-balance is sufficient to ensure that fluid can enter. How is this invasion question affected when the in situ fluid has a yield stress? Firstly, in an admittedly idealised scenario, the fluid behaves locally as a rigid solid, blocking any invasion unless the over-pressure generates stresses sufficient to locally yield the fluid around the hole. Secondly, if there is a net influx into the container it is necessary for fluid to yield and displace all the way to surface, suggesting that the height of fluid in the column is important. These are the topics we study in this paper.

Within the literature on viscoplastic fluids there are a number of works of relevance to fluid invasion and migration, although not directly to the problem we study. Regarding the migration phase, much of the literature on droplet and bubble motion is reviewed by Chhabra in the comprehensive text [8]. The question of what yield stress is sufficient to prevent migration of a bubble was addressed by Dubash & Frigaard [9,10], but the bounds derived are fairly conservative as shown by Tsamopoulos et al. [11]. There has been much recent research on bubble motion, both experimental and computational, e.g. [12–15], and to a lesser degree on droplets [16–18]. Others have studied displacement/injection flows of yield stress fluids in pipes in both *miscible* [19–23] and/or *immiscible* [24–28] scenarios. Others have studied similar flows in Hele-Shaw geometries [29,30]. Here we study invasion through a *small* hole. In her thesis, Gabard [19] studied effects of *moderate* nozzle size variations on displacement flows and in [21–23] we have studied Newtonian-viscoplastic displacement flows in pipes, with invasion hole the same size as the pipe, (i.e. initial separation of fluids via a gate valve). Thus, these studies can be interpreted as a continuous variation of hole size. However, here our concern is the actual invasion/yielding stage as motion is initiated within the yield stress fluid.

The transient start-up flow of a (weakly compressible) viscoplastic fluid caused by imposing a sudden pressure drop has been studied in [31–34] in the context of pipeline restart of waxy crude oils. In order to mobilize the gel in the pipe, a large enough pressure drop needs to be applied which is related to the pipeline length and to the fluid yield stress and bulk compressibility [35]. Waxy crude oil gel breaking mechanisms can range from adhesive (breakage at the pipe-gel interface - partial slip) to cohesive (breakdown of the internal gel structure itself - yielding) [36]. There also exist a number of works in pharmaceutical contexts that study high-speed injection of a liquid into a soft tissue mimicking needle-free jet injection of drug under the skin [37,38]. Analysis of drug jet entry into elastic polyacrylamide gels has revealed three distinct penetration stages namely *erosion*, *stagnation*, and *dispersion* [37]. The jet removes the gel at the impact site during the erosion phase leading to the formation of a distinct cylindrical hole. Thereafter, the jet comes to stagnation characterized by constant penetration depth and finally followed by dispersion of the liquid into the gel. During dispersion nearly symmetrical cracks of the injected fluid propagate within the gel. See also [38] for mathematical modeling of similar injection flows.

An outline of our paper is as follows. Section 2 introduces a setup in which to study fluid invasion and performs a dimensional analysis of the simplest setup. The experimental method is outlined in Section 3. Our main experimental results on invasion pressures and a qualitative description of fluid invasion stages are given in Section 4. Section 5 presents results of a computational study of invasion pressures, using idealised yield stress fluids, which helps to understand the transition between local yielding and a Poiseuille-type behaviour. The paper ends with a brief discussion.

2. Fluid invasion simplified

As discussed above, the objective of our study is to understand the effects of the yield stress on the invasion (i.e. penetration) stage of gas migration. Consider therefore the following simplified setup in which fluid invasion can occur. A column of an ideal incompressible yield stress fluid of height $\hat{H}$ is contained in a tank of lateral dimension $\hat{R}$, (e.g. uniform circular or rectangular cylinder). The fluid density and yield stress are denoted $\hat{\rho}$ and $\hat{\tau}_Y$, respectively. A circular orifice (hole) of radius $\hat{R}_h$ in the base of the tank (Fig. 1a) contains the invading fluid, which is assumed viscous and incompressible, with density $\hat{\rho}_i$. The invading fluid is connected via tubing to a large reservoir (Fig. 1b) that is maintained at a height $\hat{z}_R$. The reservoir height is controlled to ensure that the pressure $\hat{P}_h$, within the invading fluid orifice at the entry to the tank, is $\hat{P}_h \geq \hat{\rho}\hat{g}\hat{H}$. The question we wish to address is whether or not the invading fluid is able to penetrate into the static gelled column?

For simplicity it is assumed that $\hat{\rho}_i = \hat{\rho}$, so that buoyancy forces do not play any role in the flow. Equally, we assume that the two fluids are completely miscible, so as to neglect capillary effects. In order to penetrate into the gelled column it is clear that the visco-plastic fluid must yield. If $\hat{P}_h = \hat{\rho}\hat{g}\hat{H}$, there is no driving pressure and we may expect there to be no flow. Consider conceptually an experiment in which $\hat{z}_R$ is progressively and slowly increased, e.g. as in Fig. 1b. We expect that at some height we have sufficiently increased $\hat{P}_h > \hat{\rho}\hat{g}\hat{H}$, such that fluid penetration occurs, causing the fluid in the tank to yield and flow. The invasion pressure $\hat{P}_i$ is defined as the value of $\hat{P}_h$ at which fluid penetration first occurs.

Evidently, we expect that $\hat{P}_i$ depends on the static pressure in the yield stress fluid at the base of the tank, and thus on $\hat{\rho}$, $\hat{g}$ and $\hat{H}$. As yielding is involved, $\hat{\tau}_Y$ also naturally affects the flow. However, if we only consider the process of yielding and ignore what may happen afterwards, other rheological parameters should not affect $\hat{P}_i$. We must also consider the two geometric parameters: $\hat{R}$ and $\hat{R}_h$.

Following a dimensional analysis and subtracting the static pressure field everywhere, we find that

$$P_i = \frac{\hat{P}_i - \hat{\rho}\hat{g}\hat{H}}{\hat{\tau}_Y} = f(H, r_h), \tag{1}$$

where $H = \hat{H}/\hat{R}$ and $r_h = \hat{R}_h/\hat{R}$, i.e. the scaled invasion pressure should depend only on the dimensionless height of the yield stress fluid column and on the hole radius, i.e. 2 dimensionless parameters define P_i. Note that in this analysis, by considering only an ideal visco-plastic fluid (e.g. Bingham, Casson, Herschel-Bulkley, etc) we do not allow for other mechanical behaviours to influence the yielding process, e.g. elasto-plastic behaviour, thixotropy, etc. This simplification is purely to provide a framework with which to design our experiments and understand our results.

3. Experimental description

To explore the flow described in Section 2, we constructed a simple experiment as follows. Experiments were performed in a long Plexiglas cylinder of radius $\hat{R} = 3.175$ cm (1.25″) and height $\hat{H}_C = 63.5$ cm (25″), with sealed base. The Plexiglas cylinder was

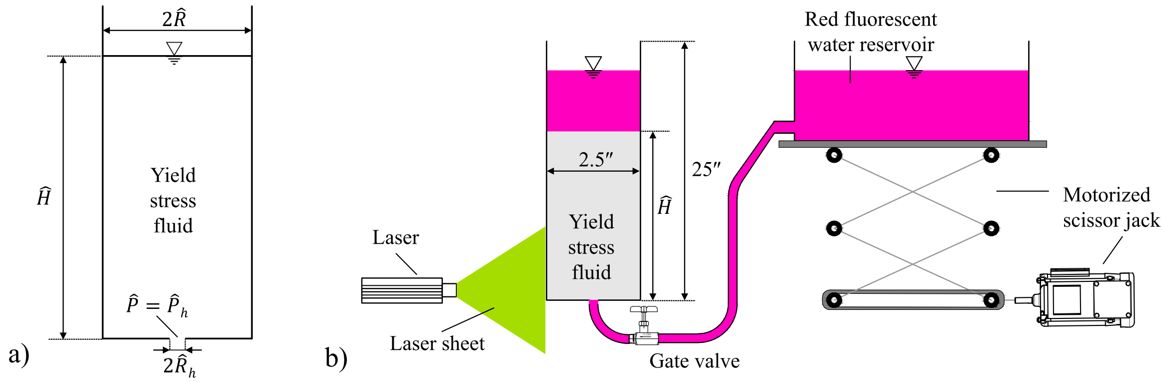

Fig. 1. Schematic setup: (a) conceptual problem; (b) experimental apparatus.

immersed in a rectangular tank filled with a glycerin solution, prepared to match the refractive index of the Plexiglas, hence minimizing optical distortion.

The cylinder is filled with a Carbopol EZ-2 solution and water invades through a hole positioned in the centre of the base, of radius $\hat{R}_h = 0.3175$ mm. To balance atmospheric pressure we control the injection pressure $\hat{P}_h$ with a manometer arrangement. The net injection pressure is then regulated by the difference in height between the carbopol column and a water reservoir; see Fig. 1b. Using this design instead of a pressure regulator, leads to elimination of both atmospheric pressure and hydrostatic pressure. In order to enhance experimental repeatability at smaller heights of carbopol, we added water on top of the carbopol column so that the total height of fluid column remained constant in each experiment, (see Section 3.2). The precision of our pressure control system is 0.1μm of water, which means a static pressure of 10^{-3}Pa, controlled by the height of the water tank via the automatic scissor jack system. The surface height measurement in the water tank is visual, with lower precision.

We use the planar Laser-Induced Fluorescence (planar-LIF) technique to measure instantaneous whole-field concentration maps of the invading fluid (water with red fluorescene). A 532 nm green laser light sheet illuminates the center plane of the tank and excites the fluorescene. The experiments were recorded by two cameras, one with 16 mm compact Fixed Focal Length Lens to record the small field of view of 2.5 × 3 cm^2, around the hole and another for recording a larger propagation field of the invaded fluid. The former one is recording with 8 frames per seconds at 0.8 megapixels and the invaded fluid propagation is recorded by a video camera at 720 pixel resolution with 60 frames per second, giving a spatial resolution of ≈10–15 pixels per mm.

With fixed hole size and cylinder radius, the parameters expected to be relevant to the experiments are the aspect ratio of the column and the yield stress of the invaded fluid, see (1). Thus, to study the effects of these parameters on the invasion pressure, we have performed experiments with a variety of concentrations of carbopol over many different heights of the carbopol column.

3.1. Fluid characterization

The in-situ (invaded) fluid was a solution of Carbopol EZ-2 (Noveon Inc). According to the desired concentration, a small amount of Carbopol EZ-2 was mixed with water and then neutralized by stirring in an appropriate amount of 0.1 g/l of sodium hydroxide (NaOH) for 24 hours. The concentration and pH of the solution mainly determine the rheological properties of the fluid. In order to avoid thixotropic and evaporation effects, a new batch of carbopol was made for each day of the experiment, using identical preparation protocols. Before starting each experiment, a series of controlled shear rate rheological measurements were conducted using a Gemini HR nano rheometer (Malvern Instruments), at 20 °C, representing the laboratory temperature.

Table 1
Rheological measurements of carbopol solutions used in the experiments.

Fluid (wt/wt)	Shear rate range $\hat{\dot{\gamma}}$ (s^{-1})	Yield Stress $\hat{\tau}_Y$ (Pa)	PH
Carbopol 0.15%	0.001–0.1	4.3–5.9	6.5–7.05
Carbopol 0.16%	0.001–0.1	6.2–7.3	6.5–7.05
Carbopol 0.17%	0.001–0.1	7.06–8.53	6.5–7.05

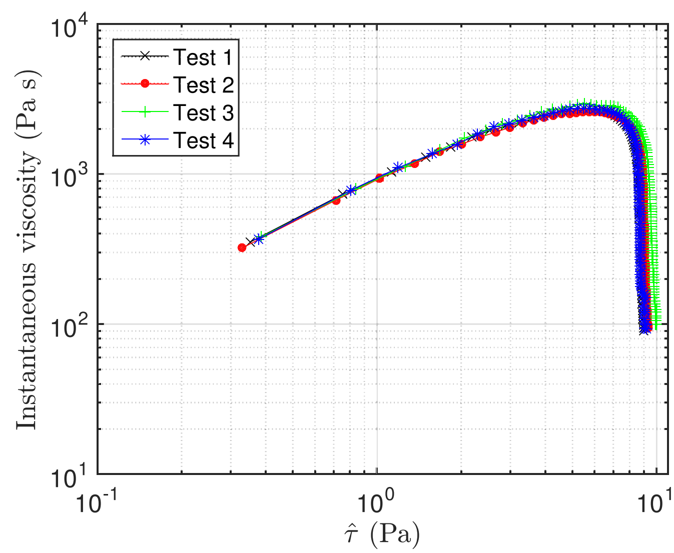

Fig. 2. Example flow curves for 4 tests using $C = 0.15\%$ (wt/wt) carbopol solution. The instantaneous viscosity technique is used to estimate the yield stress of the solution.

Shear rate sweeps over the range of 0.001–0.1 s^{-1} were conducted, with data collected for 100 points at each shear test. To negate potential elastic effects, the time step between each shear rate measurement was set to be 7 s, including delay and integration time. Three different carbopol concentrations were used, as outlined in Table 1. For each carbopol the yield stress was estimated using the maximal instantaneous viscosity method [39]. A representative example of using this method is shown in Fig. 2 for $C = 0.15\%$ carbopol. These tests were performed 4 times for each sample, with a high degree of repeatability, but nevertheless there is a significant range of maximum $\hat{\tau}$. The carbopol concentrations were limited both above and below for practical reasons. Too low a concentration resulted in a very diffuse interface and weak yield stress. The issue here is that yield stress measurement is relatively low precision and we scale with the yield stress in our dimensional analysis. Too high a concentration results in a large yield stress, which causes problems with the filling protocol (see below).

3.2. Experimental evolution, calibration and repeatability

Our initial experimental focus was on gas invasion. With the intention to investigate this in a small lab-scale experiment we identified the following stresses that would influence: (i) atmospheric pressure (10^5 Pa); (ii) static pressures ($\sim$10 cm = $O(10^3)$ Pa); (iii) yield stresses ($\sim O(10^2)$Pa); (iv) capillary stresses (depending on hole size, $\sim$ O(10–10^2) Pa); (v) buoyancy stresses. It became apparent that in order to investigate yielding we would need to impose a pressure differential of $\sim O(10^2)$ Pa, and hence control for stresses of comparable and larger magnitude.

Elimination of atmospheric pressure effects and balancing static pressure is most easily achieved via a manometer design, such as Fig. 1b. Some initial experiments using air as the invading fluid showed that the transition from yielding (i.e. invasion) to pinch-off and migration was strongly influenced by capillary and buoyancy effects. Consequently, we decided to inject an isodense miscible Newtonian fluid, water, into the carbopol, thus eliminating capillary and buoyancy stresses. In a typical experiment, we increase the injection pressure $\hat{P}_h$ by raising the reservoir continuously. Care was taken that the increase rate was slow enough (relative to the viscous timescale in the tube connecting to the reservoir) so that the invading fluid can be considered steady: hence $\hat{P}_h$ is determined purely from hydrostatics.

Following these initial design considerations, further experimental protocols and changes followed to improve repeatability. Our first tests were in square cross-section tanks. Late stages of these experiments showed asymmetric propagation of the invading fluid. To eliminate the possibility of tank geometry affecting flow symmetry we then moved to the cylindrical tank. Next, we observed poor experimental repeatability at smaller heights of carbopol. This problem was eliminated by adding water on top of the carbopol column so that the total height of fluid column remained constant in each experiment, i.e. a height $\hat{H}$ of carbopol with a height $\hat{H}_C - \hat{H}$ of water on top. We postulate that there are some minor effects of the filling procedure that may allow for residual stresses in the gelled column. The additional static pressure of the water potentially minimizes these effects. Lastly it was found that carbopol may enter into the invasion hole and block it, prior to the start of the experiment. To avoid this: (a) the hole was machined from below to be conical through the thickness of the base, i.e. $\hat{R}_h$ is the radius of hole at the entry to the tank; (b) the tank filling procedure was carefully executed; (c) we limited the carbopol concentration to 0.17% in this study. The latter of these kept the yield stress reasonably low, so that in the event of carbopol entering the hole during filling it could be easily removed.

4. Results

We have conducted approximately 100 experiments at various $\hat{\tau}_Y$ and five different $\hat{H}$. Experiments were repeated at the same column height and carbopol concentration, typically 3–5 times to reduce variability in the results. Before presenting our general results, we describe in detail the typical experimental observations.

4.1. A typical invasion experiment

The invasion/penetration of water into carbopol, namely flow yielding/initiation, is characterized by the following stages, illustrated in Fig. 3.

1. *Mixing stage:* A very small mixed region of water-carbopol develops directly above the hole. The water is observed to mix into the carbopol, but there is no observable motion of the fluids i.e. no displacement. This stage is probably driven by either molecular diffusion or osmotic pressure. The precise extent of the region is hard to specify as it is diffuse, but a typical thickness would be $\sim$ 0.1mm.
2. *Invasion stage:* At the center of the mixed region, when the pressure is high enough, the water advances into the mixed region of the carbopol column (*invasion*). Typically the invasion takes the form of a minuscule dome appearing directly above the hole, ($\approx$0.5 mm radius). Within the dome the intensity of the LIF image is significantly brighter than in the diffuse mixing stage. The invasion pressure $\hat{P}_i$ is recorded.
3. *Transition stage:* If the pressure is not increased further, the invasion dome becomes progressively diffuse but does not grow. Therefore, the applied pressure is increased beyond the invasion pressure until the small invasion dome is observed to oscillate and becomes significantly brighter. At this point the reservoir height is held constant: the pressure ($\hat{P}_{tr}$) is not increased further. These phenomena signify the onset of a second stage of the invasion, that we have called the *transition* stage.
   During transition, the small invasion dome expands. Although there is a flow into the dome from the reservoir, the change in static pressure balance is negligible and the applied pressure at the hole $\hat{P}_{tr}$ can be regarded as constant. The expansion eventually slows as the dome expands, signalling the end of the transition stage. The interface of the dome ranges from *smooth* if the applied stress is (relatively) large, to *granular* if the applied stress is small. This surface variation is illustrated in Fig. 4.
4. *Fracture stage:* At the end of the transition stage, a small finger or non-uniformity is observed to initiate a “fracture”. This either happens at the “transition” pressure, or after a slight further increase in applied pressure (needed only if the dome remains stable at the end of transition). During the fracture stage the water advances away from the dome in a dyke-like sheet, the edge of which can both finger and branch as it advances, see Fig. 8.
5. *Arrest stage:* With no further increase in static pressure to drive the flow, eventually the invasion flow stops. Stopping is dependent on the carbopol height $H(= \hat{H}/\hat{R})$. Either the invading water penetrates fully to the surface of the carbopol (for smaller H) or it may stop before reaching the surface (larger H).

4.2. Invasion and transition stages

The critical invasion pressures for different H, over all our experiments, are plotted in Fig. 5. After an initial stage at $H \sim 1$, where the invasion pressure decreases slightly, we observe an approximately linear increase in invasion pressure with H. From a naïve macroscopic perspective, we may expect this linear increase. Assuming that the material is incompressible, it is necessary for the invading fluid to displace fluid throughout the gelled column, i.e. volume is conserved. In this scenario, a yield surface must extend to surface and hence the invasion pressure should approximately scale with H.

Although sometimes considered as such, carbopol is not an “ideal” yield stress fluid. The yielding process is not abrupt, but instead we see yielding occurring macroscopically over a stress plateau/range, across which we change from elastic strain to creep and plastic flow, eventually with nonlinear stress-strain rate characteristics; see e.g. [41]. As observed in [40], depending on the bonding strength of the material (largely controlled by carbopol concentration) either ductile-type or brittle-type failure may happen at this stress plateau. Transition pressures are also plotted in Fig. 5 and show an approximately linear increase with H. It is clear

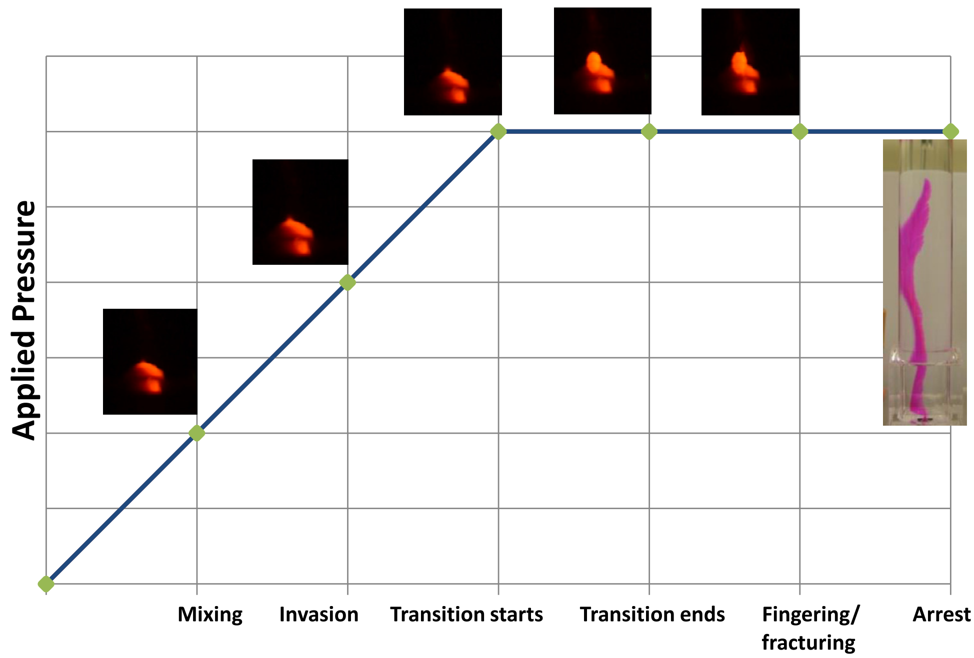

Fig. 3. Observed stages in the invasion/penetration process

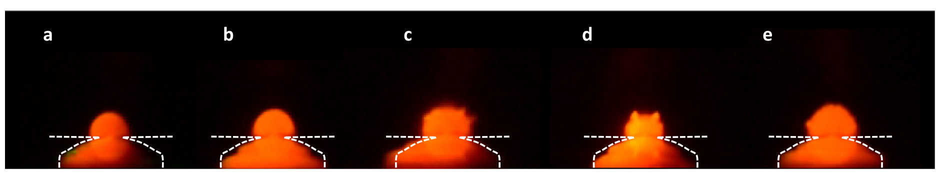

Fig. 4. Examples of dome surface shapes after "transition" showing smooth (a and b) to granular (c–e). White broken lines are a guide to the eye for the surface of the tank and machined hole.

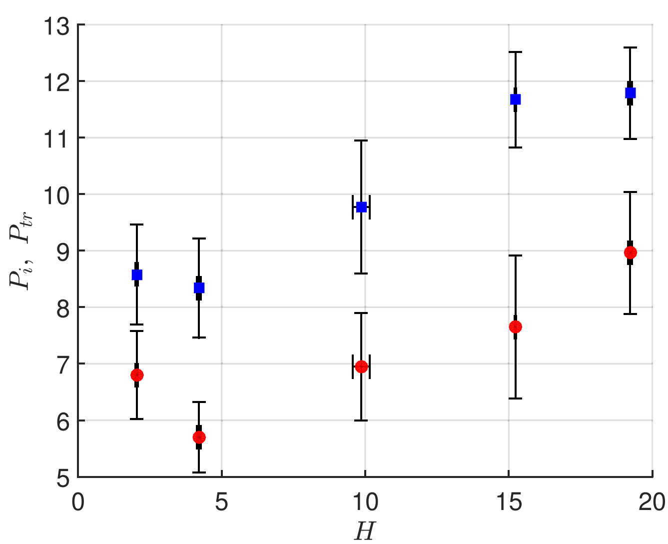

Fig. 5. Dimensionless invasion pressures P_i (red circles) and transition pressures P_{tr} (blue squares). Error bars indicate the variability of measured pressures over repeated experiments. (For interpretation of the references to colour in this figure legend, the reader is referred to the web version of this article.)

from our observations that the invasion process is not straightforward. We interpret the stage from invasion to transition as one in which the carbopol is essentially elastic. The initial invasion dome is strongly localised. As the pressure is increased and the transition pressure is attained the dome oscillation is characteristic of elastic behaviour. On the other hand, the slow transitional yielding as the dome grows under constant applied stress is characteristic of ductile-type plastic yielding. Thus, we believe that the transition pressure is indicative of this elastic-plastic threshold.

Fig. 6 displays a range of domes, for varying carbopol concentrations and H, all recorded at the end of the transition stage. Note that some image variation here is due to 2 different cameras being used. Another visual effect is that the illuminating laser sheet attenuates with depth, so that often one side of the dome appears brighter than the other. We observe that there is significant variability in dome size at each carbopol concentration and H. At least part of this is due to the unstable nature of what is being measured. It is only the oscillation of the invasion dome and a change in light intensity that signal transition: both measures can be slightly subjective. If the pressure increase is not stopped at P_{tr}, the invasion dome tends to quickly expand as the pressure increases and moves directly into the fracture mode. However, stopping the pressure increase at a suspected P_{tr} is delicate, as evidenced by the fact that some transition domes readily fracture and others need an additional pressure increase to do so. Fig. 7 shows variation in the size of the domes for different yield stress and H. There is no consistent trend apparent, with radii ranging between 1.2 and 2 mm. The initial invasion dome appears to be controlled by the hole radius ($\hat{R}_h = 0.3175$ mm) whereas final transition domes are 4-6 times the hole radius.

One interpretation of the growth and stopping of the transition domes is as a form of relaxation process, i.e. the additional pressure imposed above the invasion pressure ($P_{tr} - P_i$) causes plastic yielding and growth. As the hydrostatic balance is largely unaffected during transition, the main effect is to impose the same

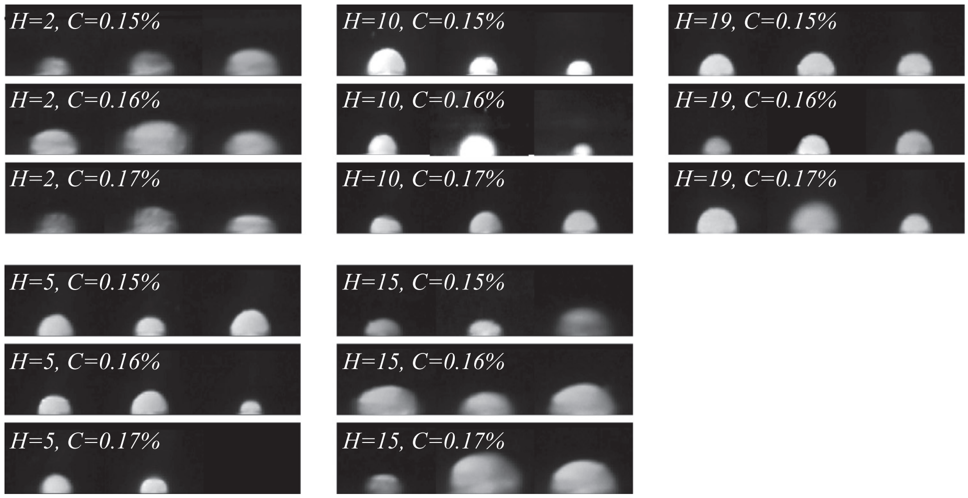

Fig. 6. Illustrations of transition dome shapes for a range of different carbopol concentrations, C, and heights, H. Snapshots for a given C and H set correspond to different experiments, repeated to reduce variability of the data.

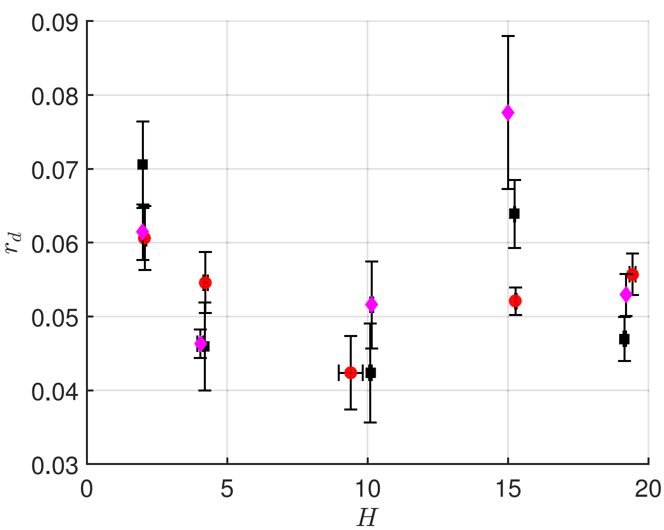

Fig. 7. Variations in transition dome size for different carbopol concentrations, marked by circles ($C = 0.15\%$), squares ($C = 0.16\%$) and diamonds ($C = 0.17\%$), and dimensionless carbopol heights, H. Each data point is obtained from more than 3 different experiments to ensure reliability.

pressure, but over a larger dome surface, thus easing the stresses in the carbopol. In this interpretation, the difference between transition and invasion pressures in Fig. 5 represents the pressure that can be relaxed in this way.

Our observation of both granular and smooth interfaces suggests a more complex and localized behaviour than that offered by macroscopic constitutive models. In the context of displacement flows, Gabard and Hulin [19,20] have observed a similar change in the rugosity of the interface in studying displacement flow of carbopol solutions from a narrow tube. With a glycerin solution displacing, smoother interfaces result from faster displacement speeds. Equally, less viscous displacing fluids led to coarser interfaces. In both cases the larger applied stress (as here) leads to the smoother interface. Note that this effect is not believed to be related to miscibility, as similar observations were made by de Souza Mendes et al. [26] in a gas-liquid displacement of carbopol. Additionally, the diffusive timescales for miscibility effects are long relative to our experimental timescales.

4.3. Post-invasion propagation

This study has focused on invasion/yielding rather than post-invasion propagation, which our ongoing work studies in more depth. Therefore, here we make a few qualitative comments only. Some examples of fractures observed are illustrated in Fig. 8. As we have seen above, the end of transition often results in coarse dome interface shapes. For such domes the initial localisation is evident. In other domes, presumably the growth/relaxation of the dome also results in some localisation of the carbopol deformation and/or stress field. In either case, the fracture propagation is characteristic of a more brittle-type failure. Observations from [40] indicate that brittle fractures are likely to happen in the presence of a localized deformation in the fluid domain at very low shear rates.

The fractures have the overall form of bladed dykes progressing upwards from the dome. The propagation itself often shows “viscous” fingering characteristics at the penetrating fracture front/edge (i.e. with branching/splitting behaviour). Visually the penetrating fronts can be diffuse and sometimes granular on small scales. The direction of propagation initially taken is not repeatable between experiments; see e.g. Figs. 8b and c, or d and e, both at very similar H and concentrations.

5. Computational predictions

As well as the experimental study described above, we have conducted a computational study, using idealised yield stress fluid models. Study of such models provides only a baseline for understanding of the invasion process. We have seen that carbopol exhibits elasto-plastic behaviours at low shear, and hence is not an ideal yield stress fluid. Therefore, in performing this type of computational study, at the outset we acknowledge that at best qualitative agreement can be expected.

5.1. The model problem and numerical method

As we are mainly interested in the invasion pressure, indicating onset of flow, rather than computing the actual velocity field and flow, we adopt the simplest model, i.e. a Bingham fluid. As most of the calculations involve stresses below the yield stress, any other ideal yield stress fluid with a von Mises yield criterion would give identical results (e.g. Casson, Herschel-Bulkley, etc). The Bingham

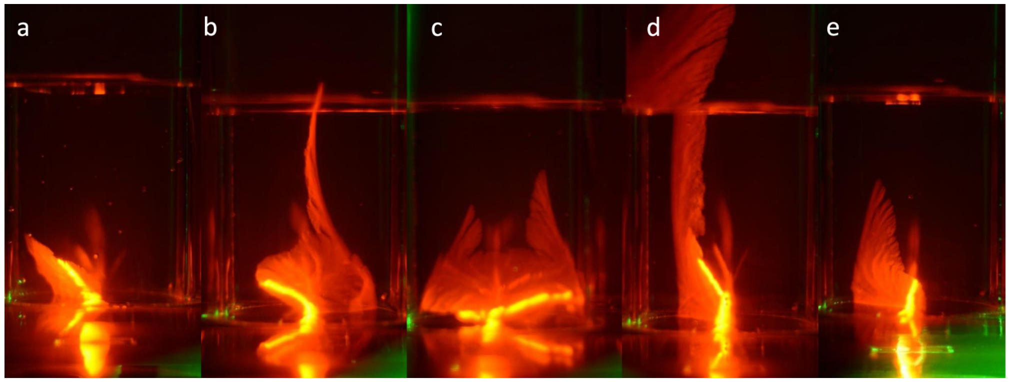

Fig. 8. Images of carbopol fractures after the transition stage for (a) $C = 0.17\%$, $\tilde{H} = 5.175$; (b) $C = 0.15\%$, $\tilde{H} = 5$; (c) $C = 0.15\%$, $\tilde{H} = 5.025$; (d) $C = 0.16\%$, $\tilde{H} = 5.1$; (e) $C = 0.16\%$, $\tilde{H} = 5.075$.

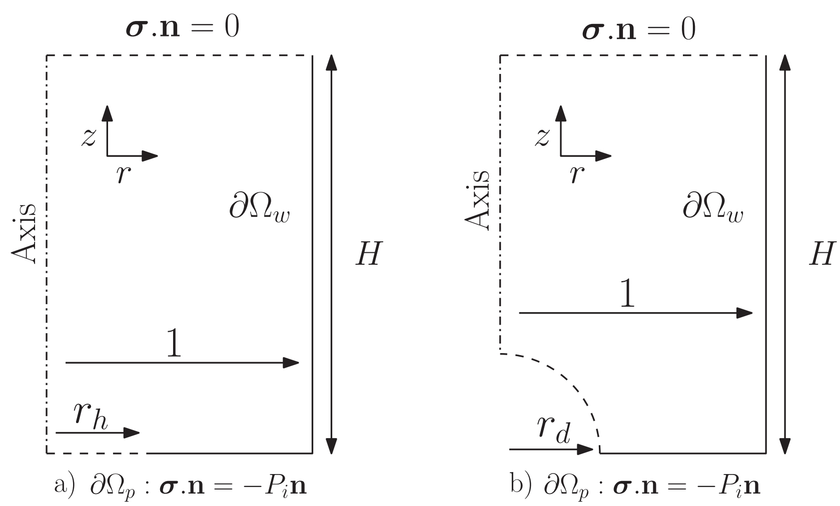

Fig. 9. Model geometry computed: (a) axisymmetric column with central flat hole at the bottom; (b) axisymmetric column with hemispherical incursion of invading fluid.

model is

$$\hat{\tau}_{ij} = \left(\hat{\mu} + \frac{\hat{\tau}_Y}{|\dot{\gamma}|}\right)\hat{\dot{\gamma}}_{ij}, \quad \Leftrightarrow \hat{\tau}_Y < |\hat{\boldsymbol{\tau}}| \tag{2a}$$

$$\hat{\dot{\boldsymbol{\gamma}}}_{ij} = 0, \quad \Leftrightarrow \hat{\tau}_Y \geq |\hat{\boldsymbol{\tau}}|. \tag{2b}$$

Here the plastic viscosity is $\hat{\mu}$, the deviatoric stress tensor is $\hat{\boldsymbol{\tau}}$ and strain rate tensor is $\hat{\dot{\boldsymbol{\gamma}}}$. The norm of the strain rate and shear stress are defined as:

$$|\hat{\boldsymbol{\tau}}| = \sqrt{\frac{1}{2}\hat{\tau}_{ij}\hat{\tau}_{ij}}, \tag{3}$$

$$|\hat{\dot{\boldsymbol{\gamma}}}| = \sqrt{\frac{1}{2}\hat{\dot{\boldsymbol{\gamma}}}_{ij}\hat{\dot{\boldsymbol{\gamma}}}_{ij}}. \tag{4}$$

On scaling stresses with the yield stress (as discussed earlier in Section 2), we can write the model in non-dimensional form as

$$\tau_{ij} = \left(1 + \frac{1}{|\dot{\gamma}|}\right)\dot{\gamma}_{ij}, \quad \Leftrightarrow 1 < |\boldsymbol{\tau}| \tag{5a}$$

$$\dot{\boldsymbol{\gamma}}_{ij} = 0, \quad \Leftrightarrow 1 \geq |\boldsymbol{\tau}|. \tag{5b}$$

Lengths have been scaled with $\hat{R}$ and velocities with $\hat{U} = \hat{\tau}_Y\hat{R}/\hat{\mu}$. The two dimensionless parameters remaining are r_h (the radius of the hole) and H (the height of the column).

We consider two similar but slightly different axisymmetric geometries, as illustrated schematically in Fig. 9. Firstly, we model directly the invasion stage of the experiment, by setting constant normal stress, $\boldsymbol{\sigma}.\boldsymbol{n} = -P_i\boldsymbol{n}$, at the flat hole, of radius r_h. Secondly, we impose constant normal stress, $\boldsymbol{\sigma}.\boldsymbol{n} = -P_i\boldsymbol{n}$, on the surface of the hemispherical dome of radius r_d. We use this setup for understanding the effects of the transition dome on the stress field. For both cases we solve the Stokes equations in the axisymmetric geometry, using constitutive laws (5). In both cases, no-slip conditions are applied at the walls, symmetry conditions are satisfied along $r = 0$, and zero stress is imposed at the top of the column.

The main difficulty with models such as the Bingham model occurs at $\dot{\boldsymbol{\gamma}} = 0$ where the effective viscosity is singular. Robust numerical algorithms for viscoplastic fluids were developed in 80's by Glowinski and coworkers [43–45], based on convex optimization methods. These algorithms produce unyielded regions with true zero strain-rate and are well-known to be superior for studying problems involving flow onset/yielding; e.g. [50]. The implementation that we use follows that in [48,49], and we have used very similar numerical codes extensively in recent work where it was important to identify unyielded regions, e.g. [46,47].

As a brief overview, two extra fields are added to the velocity and pressure: a relaxed strain rate tensor $\boldsymbol{\gamma}$ and Lagrange multiplier tensor $\mathbf{T}$ (that corresponds to the deviatoric stress). An iterative procedure consisting of three steps is repeated until the desired convergence is achieved. The first step is a Stokes flow problem with an additional source term: $\nabla \cdot [\mathbf{T} - a\boldsymbol{\gamma}]$, where $a > 0$ is an augmentation coefficient (typically $10 \leq a \leq 50$). The second and third steps are pointwise updates of the relaxed strain rate and stress Lagrange multiplier. It is known that $\boldsymbol{\gamma}$ and $\mathbf{T}$ converge to the

Please cite this article as: M. Zare et al., Invasion of fluids into a gelled fluid column: Yield stress effects, Journal of Non-Newtonian Fluid Mechanics (2016), http://dx.doi.org/10.1016/j.jnnfm.2016.06.002

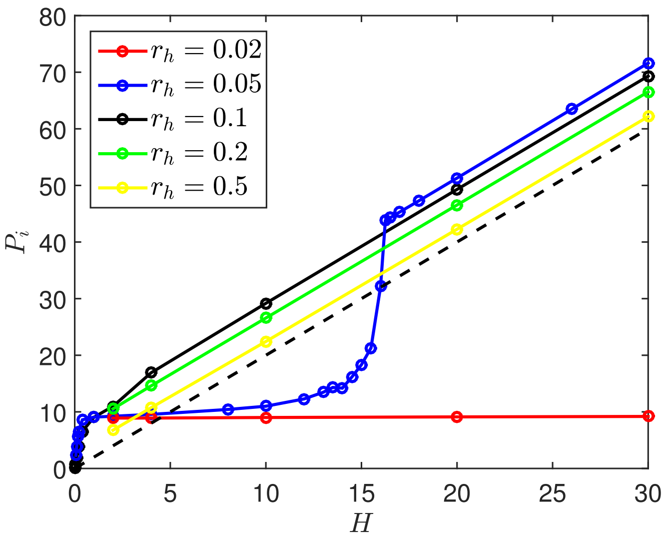

Fig. 10. Computed invasion pressures for different column height, H, and hole radii, r_h. The dashed line denotes the Poiseuille flow yield limit.

exact Bingham flow strain rate and an admissible stress field [44], as does the velocity. The nice property of the relaxed strain rate $\boldsymbol{\gamma}$ is that it becomes exactly zero in unyielded parts of the flow, at each successive iteration. Thus, when $\boldsymbol{\gamma} = 0$ for the whole domain we may infer that invasion has not happened. See Appendix A for more details of the augmented Lagrangian algorithm used.

The Stokes subproblem at each iteration is solved using the finite element method with Taylor-Hood element pair ($P_2 - P_1$) for velocity and pressure (to fulfill the inf-sup condition). The relaxed strain rate $\boldsymbol{\gamma}$ and stress multiplier $\mathbf{T}$ use linear discontinuous (P_{1d}) elements to comply with the discrete compatibility condition between velocity field and these spaces; see [48]. The mesh starts relatively coarse (40-60 points on $\partial\Omega_p$) and is refined slowly and adaptively after each converged solution. We ensure that the maximum edge size is < 0.04. Commonly used meshes can have 50,000–200,000 points and for longer columns, may reach as high as 500,000 points in size. We have implemented this algorithm using Rheolef [42], a freely available C++ finite element library developed by P. Saramito and co-workers.

A typical procedure to find the invasion pressure is as follows. First we find upper and lower bounds for the invasion pressure (twice the Poiseuille flow limiting pressure is typically a good upper bound). We then use a bisection method to find the invasion pressure. A flow is considered static (not invaded) provided that: (i) $\boldsymbol{\gamma} = 0$ in the whole domain for 100 consecutive iterations, and (ii) the relaxed strain rate is close enough to the actual strain rate i.e. $|\boldsymbol{\gamma}^n - \dot{\boldsymbol{\gamma}}(\mathbf{u}^n)|_{L2} \le 10^{-6}$. If not invaded we increase P_i following the usual bisection strategy. We continue until $\Delta P_i < 0.01$ is satisfied as a tolerance.

5.2. Results

Using the procedure described above, we have computed axisymmetric solutions, and from these have iteratively calculated the invasion pressures for a wide range of H and r_h. The results are shown in Fig. 10 and are seen to depend significantly on the hole radius r_h. For $H \lesssim 1$ the invasion pressures P_i increase from zero. This represents the transition from invasion into a shallow layer, towards invasion into a tall column.

Considering first moderate $r_h \gtrsim 0.1$, on increasing H we see that P_i increases linearly with H, for $H \gtrsim 5$. The linear increase is the same for each $r_h \gtrsim 0.1$, following the broken line marked in Fig. 10, which denotes the Poiseuille flow yield limit. More clearly, in a laminar Poiseuille flow along a length $\hat{H}$ driven by pressure drop $\Delta\hat{P}$, the wall shear stress is $= \hat{R}\Delta\hat{P}/2\hat{H}$. This must exceed the yield stress in order to flow. In the invasion context, with the scaling defined earlier, this leads to: $P_i \ge 2H$. For $H \gtrsim 5$, at the point of yielding, these flows exhibit a 2D axisymmetric region of yielded fluid fanning out from the hole and reaching the walls of the tube at a development height H_d. Above H_d the velocity field becomes essentially 1D, following a Poiseuille profile just as the fluid begins to flow/yield. As H increases the Poiseuille section grows proportionately longer, accounting for the linear increase.

Secondly, we observe in Fig. 10 that the behaviour for small r_h is quite different to that described above (see $r_h = 0.02$, ˜0.05). Evidently, as r_h decreases the inflow pressure is increasingly localised and singular. For $H > 1$ we observe a strong reduction in P_i below that of the invasion pressures for larger r_h. It appears that the fluid adopts a more localised stress distribution in this range of H. Over this range of H the fluid yields significantly below the Poiseuille flow prediction. Eventually the pressure reduction terminates at some height and thereafter the Poiseuille gradient is followed. In fact P_i is larger for smaller r_h in the Poiseuille dominated regime. For $r_h = 0.05$ (as illustrated) the Poiseuille regime is attained at $H \approx 16$. For $r_h = 0.02$ the Poiseuille regime is only attained at $H \approx 225$, i.e. as r_h is reduced, the reduction in P_i below the Poiseuille regime invasion pressure is found over an increasingly wide range of H.

To understand differences in the yielding patterns for both small and larger r_h, examples of the stress distributions are presented in Fig. 11, for $r_h = 0.05, 0.1$ at $H = 2$, i.e. at the invasion pressure. For $r_h = 0.05$ we observe that τ_{rz} and τ_{rr} change sign within a small localised dome shape. Together with and aided by non-zero $\tau_{\theta\theta}$ and τ_{zz} (of similar magnitude), we see that $|\tau| = 1$ within a small dome around the hole. This dome is isolated from the walls of the cylinder, suggesting that fluid within the dome would recirculate on yielding. This recirculation could of course entrain invading fluid from the hole, but remains a local mobilization rather than an invasion that extends to the top of the fluid column.

On the other hand, for $r_h = 0.1$, we see that although the qualitiative distribution of τ_{rz}, $\tau_{\theta\theta}$ and τ_{rr} is similar to that for $r_h = 0.05$ close to the hole, the wedge of negative shear stress τ_{rz}, now extends out from the dome near to the hole, all the way to the wall. It combines with the stress components and is nearly able to yield the fluid to surface. As H increases moderately for $r_h = 0.1$ (not shown) the shear stress increases and the Poiseuille-like distribution commences, extending along the column to surface.

To see the transition from the strongly localized stress dome into the Poiseuille flow regime at $r_h = 0.05$, Fig. 12 shows τ_{rz} and $|\tau|$ for $H = 8, 12, 15, 16, 16.25$. As we see, the stress distribution local to the hole does not change qualitatively as H increases, but does penetrate increasingly far towards the wall. Before the entire column begins to yield we can see that the shear stress adopts a 1D Poiseuille profile, e.g. for $H = 15, 16$, whereas the column only begins to displace at $H = 16.25$ (below this motion is only local to the hole).

Computed P_i for $r_h = 0.01$ (experimental value) are approximately constant over the range of experimental H, being very similar to $r_h = 0.02$ shown in Fig. 10. Comparing with the experimental results in Fig. 5 we observe 2 primary differences. First, the invasion pressures in the experiment are smaller by 10-30%. Secondly, although experimentally we see a short plateau (or decrease) at small H and then increase in P_i with H, the increase is significantly smaller than that of the Poiseuille flow gradient ($P_i = 2H$). The offset in invasion pressures is undoubtedly due partly to the constitutive law: carbopol is not a rigid solid below the yield value, but exhibits elasto-plastic behaviour that allows it to deform at lower

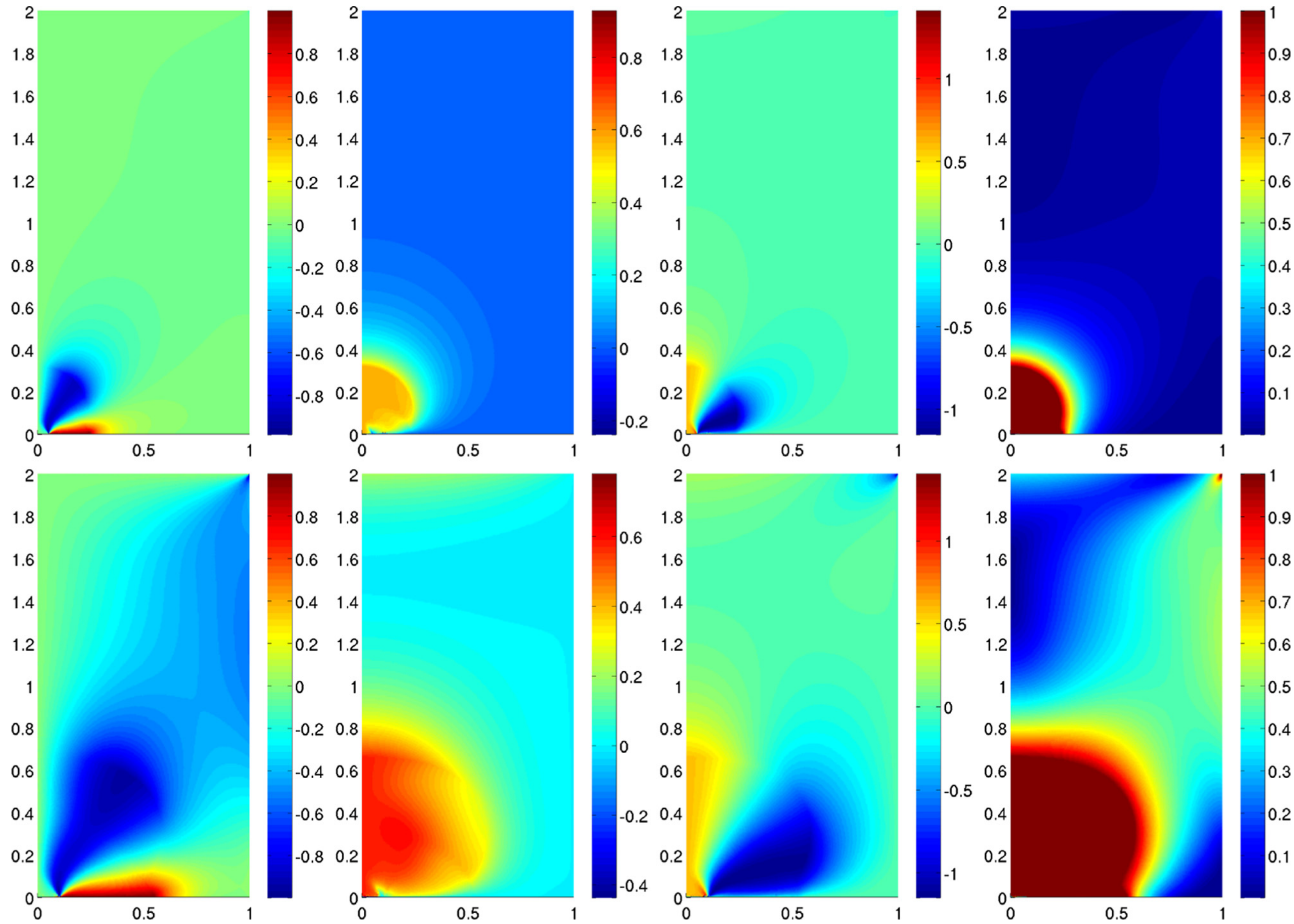

Fig. 11. Example stress fields for $H = 2$. Top row $r_h = 0.05$: τ_{rz}, $\tau_{\theta\theta}$, τ_{rr}, $|\tau|$ (left to right). Bottom row $r_h = 0.1$: τ_{rz}, $\tau_{\theta\theta}$, τ_{rr}, $|\tau|$ (left to right).

pressures than an idealised yield stress fluid. The slower increase in P_i with H (experimentally) suggests a localised stress distribution and reduction in P_i, e.g. as shown in Fig. 10 for $r_h = 0.05$.

In our experiments, following the initial very small invasion dome, the pressure is further increased until the transition pressure after which it grows at constant pressure. At the end of transition, domes are either stable or initiate fingering/fracturing. The latter mode of propagation via localisation and symmetry breaking suggests that the expanded axisymmetric dome is itself a stable configuration and that a form of stress relaxation occurs via slow growth of the dome. Initially, P_i imposed at the circular hole caused growth of the small invasion dome, (observed to be stable in the absence of further pressure increases). The pressure increase imposed, $P_{tr} - P_i$, then causes growth of the dome, at the end of which P_{tr} is imposed over the larger transition dome radius, allowing a stress field of smaller shear stress. To test the plausibility of the above description, Fig. 13 plots invasion pressures against r_d for various H, assuming that the invading pressure is imposed on a hemispherical surface of radius r_d (see Fig. 9b).

We observe that the invading pressures at small r_d attain a plateau to similar values to those for the hole. It seems that P_i increases to a maximum as r_d increases, and then slowly reduces. Computations over a wider range of r_d show that P_i approaches the Poiseuille limit at large r_d, (marked with broken horizontal lines for each H in Fig. 13). Consulting Fig. 5 it seems that the pressure increase imposed experimentally, $P_{tr} - P_i$, is in the range 1–3. Increasing the invasion pressure by ΔP =1–3, above that for $r_h = 0.01$ in Fig. 13a, indicates that the increased invasion pressure will be balanced for an increase in dome size, of somewhere in the range r_d =0.025–0.075, over the experimental range of H. We observe that this range of dome radii approximately covers the range of observed transition dome radii in Fig. 7. This suggests that the notion of the stress relaxing as the dome grows during transition is plausible.

Algorithm 1 Augmented Lagrangian algorithm for invasion

repeat

Step 1: Solve Stokes flow problem (minimization with respect to $\mathbf{u}$):

$$-a\nabla.\dot{\boldsymbol{\gamma}}(\mathbf{u}^n) = -\nabla p^n + \nabla.(\mathbf{T} - a\boldsymbol{\gamma})^{n-1}$$

$$\boldsymbol{\sigma}^n.\boldsymbol{n} = -P_i\boldsymbol{n} \text{ on } \Omega_p$$

$$\boldsymbol{\sigma}^n.\boldsymbol{n} = 0 \text{ on outlet}$$

$$\mathbf{u}^n = 0 \text{ on } \Omega_w$$

Step 2: Minimization with respect to $\boldsymbol{\gamma}$:

$$\boldsymbol{\gamma}^n = \begin{cases} 0 & \|\mathbf{T}^{n-1} + a\dot{\boldsymbol{\gamma}}(\mathbf{u}^n)\| < 1 \\ \{1 - \frac{1}{\|\mathbf{T}^{n-1}+a\dot{\gamma}(\mathbf{u}^n)\|}\}\frac{\mathbf{T}^{n-1}+a\dot{\boldsymbol{\gamma}}(\mathbf{u}^n)}{1+a} & \text{otherwise} \end{cases}$$

Step 3: Maximization with respect to T:

$$\mathbf{T}^n = \mathbf{T}^{n-1} + a(\dot{\boldsymbol{\gamma}}(\mathbf{u}^n) - \boldsymbol{\gamma}^n)$$

until $|\boldsymbol{\gamma}^n - \dot{\boldsymbol{\gamma}}(\mathbf{u}^n)| \leq 10^{-6}$ or iteration count≥5000

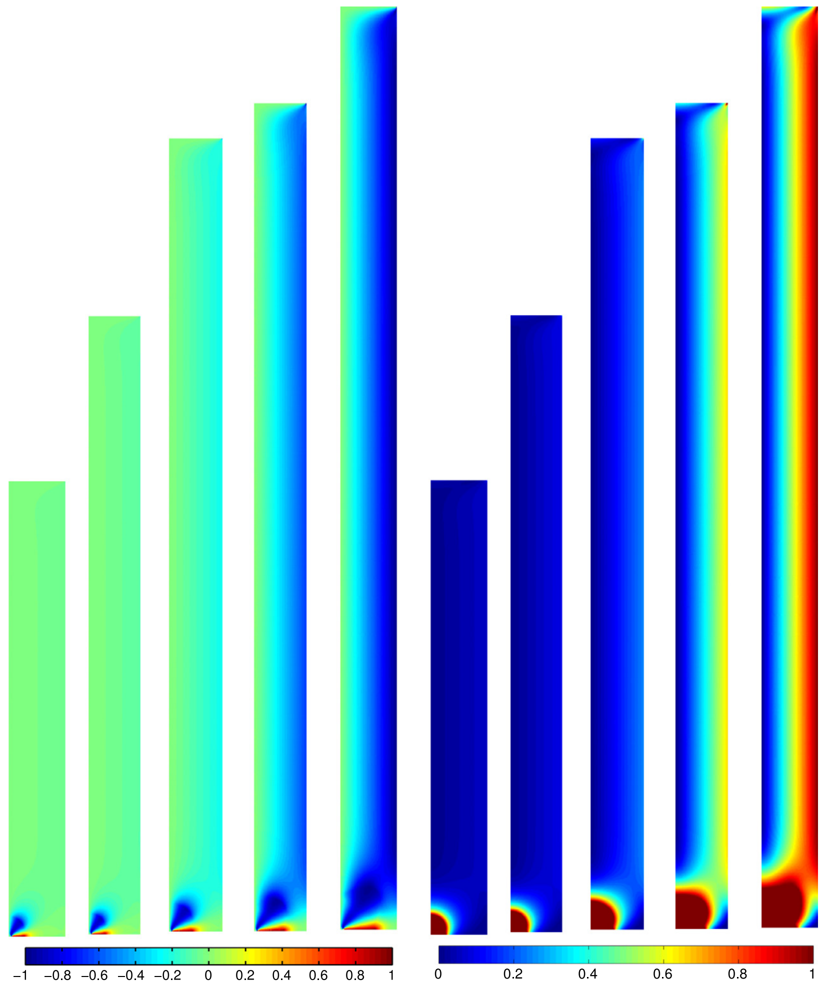

Fig. 12. Evolution of the stress fields with $H = 8$, ˜12, ˜15, ˜16, ˜16.25 for $r_h = 0.05$: left panel τ_{rz}; right panel $|\boldsymbol{\tau}|$.

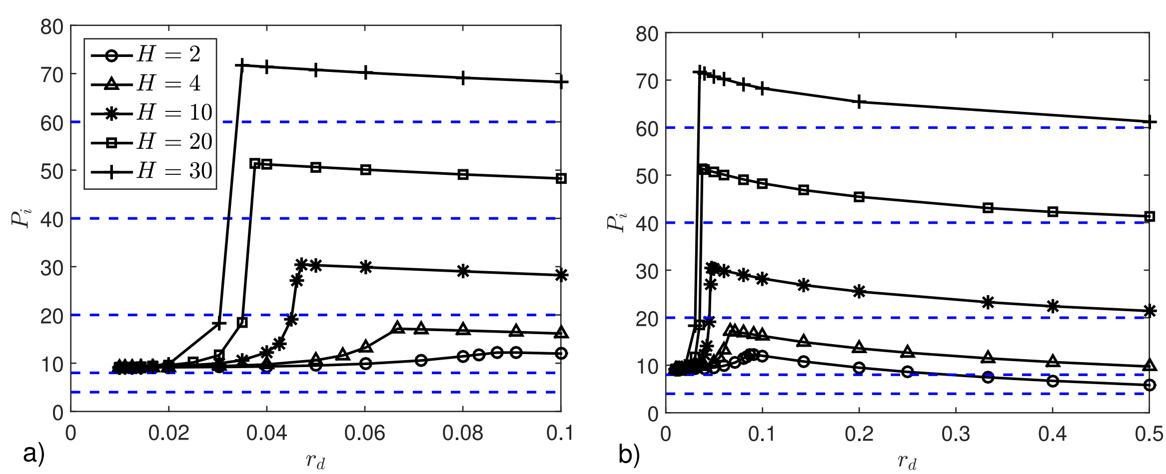

Fig. 13. Invasion pressures, for a hemispherical invading dome: (a) small r_d; (b) full range of r_d.

6. Discussion and conclusions

We have presented new results targeted at exposing the effects of the yield stress on the pressure P_i required for one fluid to invade a column of fluid, through a *small* hole. This setup was designed to simulate invasion into a well during primary cementing (or other operations when the wellbore fluid is stationary), for relatively low porosity reservoirs where pores may be considered isolated. Water was used in place of gas (to eliminate buoyancy and capillary effects) and the invading fluid was a carbopol gel. Approximately 100 experiments were performed, repeatedly covering 3 different carbopol concentrations and various heights of column. This was supplemented by a computational study.

For low column heights $H \sim 1$ ($\hat{H} \sim \hat{R}$) there is little effect of H, but as H increases we observe a steady approximately linear increase in P_i over the experimental range. Dimensionally, P_i

measures the invasion over-pressure (i.e. pressure above the hydrostatic pressure in the fluid column), scaled with the yield stress. Thus, our results show approximately linear increase in invasion over-pressure with $\hat{H}$. Also the invasion over-pressure increases linearly with the yield stress, as follows simply from the scaling adopted.

The experiments show significant variability, hence the repetition at each height and carbopol concentration, despite considerable evolution in the experimental procedure to reduce this. For example, we have carefully implemented protocols for fluid preparation, tank filling, eliminating invasion hole plugging, etc..., and have eliminated buoyancy, capillary, static and atmospheric pressures via our experimental design. The remaining variability stems from the fact that we are measuring an isolated onset event in a dynamically evolving process, and that this event is identified phenomenologically by the appearance of a minuscule invasion dome.

A number of interesting stages have been observed during the experiments: *mixing, invasion, transition, fracture* and *arrest*. The last of these we are currently studying in more depth as our setup and measurements were targeted at invasion. The passage from invasion to transition pressure seems to represent elastic-plastic yielding close to the invasion hole. The initial growth of the transition dome and then slowing of growth (in cases where the fracture does not start immediately) suggests a relaxation of the stress field, due to the overpressure now being applied over a larger area. We have seen that the expanding dome interface can be either relatively smooth or granular. This does not appear to have any bearing on the stability of the transition dome: either may be stable or unstable. Invasion and transition domes are approximately axisymmetric. Fracture initiation and propagation represent a departure from symmetry, probably due to either a local defect or a non-uniformity of the stress-field.

The computational study has covered a range of invasion hole sizes and dimensionless H. The computed invasion pressures follow similar qualitative trends to the experiments but are themselves over-predicted. This is probably due to the ideal visco-plastic (Bingham) law that we have implemented. The computations also reveal that the invasion pressures for small r_h increase relatively slowly with $H > 1$. This is tied into the occurrence of a local dome-like region of yielding close to the hole, i.e. the invasion overpressure first causes fluid to yield and recirculate locally within a dome shape, that appears analogous to those observed during the transition stage.

As H is significantly increased, for small r_h, the increase in P_i eventually generates sufficient stress to reach the walls of the cylinder. After this the invasion process changes from a local phenomena to a global one, in which resistance of the fluid occurs on the scale of the cylinder. More specifically, there remains an $O(1)$ region close to the hole within which the magnitude of the deviatoric stresses components are all significant. The stresses generally decrease away from the hole, but at sufficiently large H yielded fluid does extend to the wall. Above this local near-hole region, the fluid adopts essentially a Poiseuille profile, with linearly decreasing shear stress from centre to wall. Hoop and extensional stresses, which are important in the near-hole region, decay in the Poiseuille region as H is increased.

We further observe that the invasion pressure increase proceeds in parallel to the Poiseuille prediction ($P_i = 2H$) both for small r_h at sufficiently large H and for larger r_h. For the latter there is no range of H for which yielding is local and isolated, instead the Poiseuille regime is entered immediately. Returning to the experimental results, the invasion pressures increases at a rate that is significantly below $P_i = 2H$. This, the hole size and the phenomena observed, all suggest that our experiments are fully in the local regime of invasions. The initial domes are approximately axisymmetric and apart from more complex constitutive behaviour the computational and experimental results present a coherent picture.

Regarding the cementing process, a few aspects appear relevant. Firstly, the complex behaviour of P_i with H and secondly the change from local to non-local invasion. Here we neglect effects of any filtercake that may have formed during drilling. Although H is very large in the wellbore setting, pore size is also very small. Taking a typical annular gap as the global scale, pore sizes in the submicron range are very likely to invade locally ($r_h < 0.0001$ even for large H). This will also depend in a significant way on the porosity, which can also be interpreted as r_h, i.e. at larger porosity values pores can no-longer be considered as isolated: local invasion domes influence adjacent pores. Our computed results suggest that in the cylindrical geometry this happens for $r_h \gtrsim 0.1$.

Secondly, a different perspective on local/non-local yielding comes from the observations of smooth and granular surfaces in our transition domes. Here the scale of the granularity appears to be in the range of $1 - 100\tilde{}\mu m$, which may be related to the carbopol gel microstructure and its stress response on this scale. In the well, cement slurries are in reality fine suspensions and pore sizes in tight rocks extend down to the scale of the suspension microstructure, (indeed in such rocks it is not uncommon to consider Knudsen effects on porous media flows). Thus, local invasion on the scale of the slurry microstructure is likely to be the norm in cementing and this requires separate study using real cements.

Thirdly, the influence of the yield stress in linearly increasing invasion over-pressure is useful, if also anticipated. If the invasion is local then the critical point is that it may occur at significantly lower pressures than those predicted from non-local analyses, e.g. predicting flow in the annular gap. If however yielding is local, with recirculation of fluids close to the pore opening, many other effects may influence the potential and mechanism for annular fluid to exchange with the pore fluid, and the timescale for that exchange, e.g. buoyancy, capillarity, diffusion, osmotic pressure... These effects have not been studied here. In the same context, note that here we have tried to eliminate local variability in our experiments, but in any cement placement process (and in the drilling process) the wellbore is over-pressured. Thus, yield stress fluid is forced into the pores, *filtercake/skin* typically forms close to the borehole, and these effects may in practical situations be the main influence of the yield stress on the actual invasion stage.

Finally, in the above context - if we are to assume that local invasion occurs and that local gas streams coalesce, an interesting fluid mechanics problem to consider would be the propagation of a large gas stream upwards through an inclined annulus of stationary yield stress fluid. Although in our simple setup we have shown the relevance of Poiseuille flow-like bounds, in inclined eccentric annuli the gas path is less predictable and may exchange/by-pass in situ fluids as it rises up the annulus.

Acknowledgements

This research has been carried out at the University of British Columbia, supported financially by the British Columbia Oil and Gas Commission, by BC-OGRIS (project EI-2016-09) as well as partly by NSERC and Schlumberger through CRD project 444985-12.

Appendix A. The augmented Lagrangian method

In Section 5.1 it was mentioned that a bisection algorithm has been used to find the invasion pressure. The objective function is an evaluation of $\max_{\Omega}||\gamma||$ and we compute the maximal P_i for which $\max_{\Omega}||\gamma|| = 0$. To find $\boldsymbol{\gamma}$ at each step, we solve the flow problem in the column of fluid for given invasion pressure P_i. We use the augmented Lagrangian method at each step which itself consists of fixed point iterations through 3 steps of an Uzawa algorithm. These 3 steps find the solution of a saddle-point problem with respect to the three variables $\mathbf{u}$, $\boldsymbol{\gamma}$ and $\mathbf{T}$ as follows.

The variable $\boldsymbol{\gamma}$ and $\mathbf{T}$ are the relaxed strain rate and stress Lagrange multiplier respectively as mentioned before. By iterating through these steps these variables converge to the real strain rate and deviatoric stress of the flow. In step 2 we observe that the relaxed strain rate is set exactly to zero if the stress approximation at that step does not exceed the yield stress (here unity). Thus, when converged $\max_{\Omega} ||\gamma|| = 0$ implies that the fluid is everywhere unyielded. These iterations usually converge very fast (tens of iterations) for non invading pressures and $\boldsymbol{\gamma} = 0$ is obtained through the whole domain.

References

[1] R.B. Stewart, .F.C. Schouten, Gas invasion and migration in cemented annuli: Causes and cures, SPE Drill. Eng. 3 (01) (1988) 77–82.
[2] F. Sabins, M.L. Wiggins, Parametric study of gas entry into cemented wellbores, in: SPE Annual Technical Conference and Exhibition, 1994. SPE paper 28472.
[3] E.B. Nelson, D. Guillot, Well Cementing, 2nd edn., Schlumberger, 2006.
[4] C.E. Bannister, G.E. Shuster, L.A. Wooldridge, M.J. Jones, A.G. Birch, Critical design parameters to prevent gas invasion during cementing operations, in: SPE Annual Technical Conference and Exhibition, 1983. SPE paper 11982.
[5] P.R. Cheung, R.M. Beirute, Gas flow in cements, J. Petrol. Technol. 37 (06) (1985) 1–41.
[6] M.E. Chenevert, B.K. Shrestha, Chemical shrinkage properties of oilfield cements, SPE Drill. Eng. 6 (01) (1991) 37–43.
[7] M. Norton, W. Hovdebo, D. Cho, M. Jones, S. Maxwell, Surface seismic to microseismic: an integrated case study from exploration to completion in the montney shale of NE british columbia, canada, SEG Annual Meeting, 2010.
[8] R.P. Chhabra, Bubbles, Drops, and Particles in Non-Newtonian Fluids, 2nd edn., CRC Press, 2006.
[9] N. Dubash, I. Frigaard, Conditions for static bubbles in viscoplastic fluids, Phys. Fluids 16 (12) (2004) 4319–4330.
[10] N. Dubash, I. Frigaard, Propagation and stopping of air bubbles in carbopol solutions, J. Non-Newt. Fluid Mech. 142 (1) (2007) 123–134.
[11] J. Tsamopoulos, Y. Dimakopoulos, N. Chatzidai, G. Karapetsas, M. Pavlidis, Steady bubble rise and deformation in newtonian and viscoplastic fluids and conditions for bubble entrapment, J. Fluid Mech. 601 (2008) 123–164.
[12] D. Sikorski, H. Tabureau, J.R. de Bruyn, Motion and shape of bubbles rising through a yield-stress fluid, J. Non-Newt. Fluid Mech. 159 (2009) 10–16.
[13] N. Mougin, A. Magnin, J.M. Piau, The significant influence of internal stresses on the dynamics of bubbles in a yield stress fluid, J. Non-Newt. Fluid Mech. 171 (2012) 42–55.
[14] Y. Dimakopoulos, M. Pavlidis, J. Tsamopoulos, Steady bubble rise in Herschel Bulkley fluids and comparison of predictions via the augmented lagrangian method with those via the papanastasiou model, J. Non-Newt. Fluid Mech. 200 (2013) 34–51.
[15] A. Tran, M.L. Rudolph, M. Manga, Bubble mobility in mud and magmatic volcanoes, J. Volcanol. Geotherm. Res. 294 (2015) 11–24.
[16] A. Potapov, R. Spivak, O.M. Lavrenteva, A. Nir, Motion and deformation of drops in a Bingham fluid, Ind. Eng. Chem. Res. 45 (2006) 6985–6995.
[17] O.M. Lavrenteva, Y. Holenberg, A. Nir, Motion of viscous drops in tubes filled with yield stress fluid, Chem. Eng. Sci. 64 (22) (2009) 4772–4786.
[18] A. Maleki, S. Hormozi, A. Roustaei, I. Frigaard, Macro-size drop encapsulation, J. Fluid Mech. 769 (2015) 482–521.
[19] C. Gabard, Etude de la stabilité de films liquides sur les parois d'une conduite verticale lors de l'ecoulement de fluides miscibles non-newtoniens, These de l'Universite Pierre et Marie Curie, Orsay, France, 2001 (PhD thesis).
[20] C. Gabard, J.P. Hulin, Miscible displacement of non-newtonian fluids in a vertical tube, Eur. Phys. J. E 11 (3) (2003) 231–241.
[21] S.M. Taghavi, K. Alba, M. Moyers-Gonzalez, I.A. Frigaard, Incomplete fluid-fluid displacement of yield stress fluids in near-horizontal pipes: experiments and theory, J. Non-Newt. Fluid Mech. 67 (2012) 59–74.
[22] K. Alba, S.M. Taghavi, J.R. Bruyn, I.A. Frigaard, Incomplete fluid-fluid displacement of yield-stress fluids. Part 2. Highly inclined pipes, J. Non-Newt. Fluid Mech. 201 (2013) 80–93.
[23] K. Alba, I.A. Frigaard, Dynamics of the removal of viscoplastic fluids from inclined pipes, J. Non-Newt. Fluid Mech. 229 (2016) 43–58.
[24] A.J. Poslinski, P.R. Oehler, V.K. Stokes, Isothermal gas-assisted displacement of viscoplastic liquids in tubes, Polym. Eng. Sci. 35 (11) (1995) 877–892.
[25] Y. Dimakopoulos, J. Tsamopoulos, Transient displacement of a viscoplastic material by air in straight and suddenly constricted tubes, J. Non-Newt. Fluid Mech. 112 (2003) 43–75.
[26] P.R. de Souza Mendes, E.S.S. Dutra, J.R.R. Siffert, M.F. Naccache, Gas displacement of viscoplastic liquids in capillary tubes, J. Non-Newt. Fluid Mech. 145 (1) (2007) 30–40.
[27] D.A. de Sousa, E.J. Soares, R.S. de Queiroz, R.L. Thompson, Numerical investigation on gas-displacement of a shear-thinning liquid and a visco-plastic material in capillary tubes, J. Non-Newt. Fluid Mech. 144 (2) (2007) 149–159.
[28] R.L. Thompson, E.J. Soares, R.D.A. Bacchi, Further remarks on numerical investigation on gas displacement of a shear-thinning liquid and a visco-plastic material in capillary tubes, J. Non-Newt. Fluid Mech. 165 (7) (2010) 448–452.
[29] A. Lindner, P. Coussot, D. Bonn, Viscous fingering in a yield stress fluid, Phys. Rev. Lett. 85 (2) (2000) 314.
[30] J.V. Fontana, S.A. Lira, J.A. Miranda, Radial viscous fingering in yield stress fluids: Onset of pattern formation, Phys. Rev. E. 87 (1) (2013) 013016.
[31] G. Vinay, Modélisation du redemarrage des écoulements de bruts parafiniques dans les conduites pétrolieres, These de l'Ecole des Mines de Paris, Paris, France, 2005 PhD thesis.
[32] G. Vinay, A. Wachs, J.F. Agassant, Numerical simulation of weakly compressible Bingham flows: the restart of pipeline flows of waxy crude oils, J. Non-Newt. Fluid Mech. 136 (2) (2006) 93–105.
[33] G. Vinay, A. Wachs, I. Frigaard, Start-up transients and efficient computation of isothermal waxy crude oil flows, J. Non-Newt. Fluid Mech. 143 (2) (2007) 141–156.
[34] A. Wachs, G. Vinay, I. Frigaard, A 1.5d numerical model for the start up of weakly compressible flow of a viscoplastic and thixotropic fluid in pipelines, J. Non-Newt. Fluid Mech. 159 (1) (2009) 81–94.
[35] I. Frigaard, G. Vinay, A. Wachs, Compressible displacement of waxy crude oils in long pipeline startup flows, J. non-Newt. Fluid Mech. 147 (1) (2007) 45–64.
[36] H.S. Lee, P. Singh, W.H. Thomason, H.S. Fogler, Waxy oil gel breaking mechanisms: adhesive versus cohesive failure, Energy & Fuels 22 (2008) 480–487.
[37] J. Schramm-Baxter, J. Katrencik, S. Mitragotri, Jet injection into polyacrylamide gels:investigation of jet injection mechanics, J. Biomech. 37 (2004) 1181–1188.
[38] K. Chen, H. Zhou, J. Li, G.J. Cheng, Modeling and analysis of liquid penetration into soft material with application to needle-free jet injection, in: In Proceedings of 3rd International Conference on Bioinformatics and Biomedical Engineering, 2009. ICBBE 2009 doi:10.1109/ICBBE.2009.5163069
[39] P.S. Mendes, E.S. Dutra, Viscosity function for yield-stress liquids, Appl. Rheol. 14 (6) (2004) 296–302.
[40] J.E. Reber, L.L. Lavier, N.W. Hayman, Experimental demonstration of a semi-brittle origin for crustal strain transients, Nat. Geosci. 8 (2015) 712–715.
[41] C. Tiu, J. Guo, P.H.T. Uhlherr, Yielding behaviour of viscoplastic materials, J. Ind. Eng. Chem. 12 (5) (2006) 653–662.
[42] P. Saramito, Efficient c++ finite element computing with rheolef, 2012, http://wwwljk.imag.fr/membres/Pierre.Saramito/rheolef/rheolef.pdf CNRS-CCSD ed.
[43] M. Fortin, R. Glowinski, Augmented Lagrangian Methods, North-Holland, 1983.
[44] R. Glowinski, Numerical Methods for Nonlinear Variational Problems, Springer-Verlag, 1983.
[45] R. Glowinski, P.l. Tallec, Augmented Lagrangian and operator-splitting methods in nonlinear mechanics, SIAM (1989).
[46] A. Roustaei, I.A. Frigaard, The occurrence of fouling layers in the flow of a yield stress fluid along a wavy-walled channel, J. Non-Newt. Fluid Mech. 198 (2013) 109–204.
[47] A. Roustaei, A. Gosselin, I.A. Frigaard, Residual drilling mud during conditioning of uneven boreholes in primary cementing.part 1: rheology and geometry effects in non-inertial flows, J. non-Newt. Fluid Mech. 220 (2014) 87–98.
[48] P. Saramito, N. Roquet, An adaptive finite element method for viscoplastic fluid flows in pipes, Comp. Meth. Appl. Mech. Eng. 190 (2001) 5391–5412.
[49] N. Roquet, P. Saramito, An adaptive finite element method for Bingham fluid flows around a cylinder, Comp. Meth. Appl. Mech. Engng. 192 (2003) 3317–3341.
[50] R. Glowinski, A. Wachs, On the numerical simulation of viscoplastic fluid flow, in: Handbook Numerical Analysis, vol. 16, 2011, pp. 483–717.